Control and Monitoring of a High Recovery Reverse Osmosis Desalination Process

Charles W. McFall, Alex Bartman, Panagiotis D. Christofides,* and Yoram Cohen

Department of Chemical and Biomolecular Engineering, University of California, Los Angeles, California 90095

Model-based control and monitoring such as feed-forward/feedback control, fault detection and isolation (FDI), and fault-tolerant control (FTC) techniques that utilize Lyapunov-based control laws are implemented on a high recovery reverse osmosis desalination plant model. A detailed mathematical model of a high recovery reverse osmosis plant is developed. This model incorporates the large spatial variations of concentration and flow rate that occur in membrane units during high recovery operation. Bounded nonlinear feedback and feed-forward controllers are developed and applied to this system. The application of these controllers with FDI and FTC is demonstrated in the context of a high recovery reverse osmosis process simulation. The first set of simulations demonstrates the ability to compensate for the effects of large time-varying disturbances in the feed concentration on specific process outputs with and without feed-forward control. The second set of simulations demonstrates the ability of FDI and FTC techniques to recover desired plant operation subject to actuator failures.

1. Introduction

System automation and reliability are crucial elements of any modern reverse osmosis (RO) plant. The operational priorities are personnel safety and product water quality, while also meeting environmental and economic demands. It is highly desirable to operate RO processes at high recovery, where most of the feedwater volume is processed to low salinity product water, due to decreased environmental and economic costs associated with brine disposal.[18,27] Automated RO plants that operate at high recovery, however, can become more vulnerable to disturbances in feedwater quality, total dissolved solids (TDS) concentrations, and temperature. Such disturbances often appear in usual feedwater sources, due to temporal and spatial variations.[2,9] These disturbances can cause undesirable behavior in product flow rate, internal system pressure, and brine flow rate. Automated RO systems are also vulnerable to actuator failures, such as actuated pumps or valves that may not operate in the expected manner. It is critical to be able to quickly pinpoint the location of a fault and take action before it propagates and disturbs overall RO plant operation.

Several contributions have been made in the literature to automatic control of RO systems. The first paper which proposed an effective closed-loop control strategy for RO utilized multiple single-input single-output (SISO) classical (i.e., proportional, integral, derivative (PID)) control loops.[3] Within a model-based control setting, step tests were used to perform system identification, resulting in a model that is a linear approximation around the operating point. The control algorithm of model predictive control (MPC) was applied to the resulting linear model.[1,29] Experimental system identification and MPC applications can also be found in the literature.[4,7] Additional work[17,20] implements feedback control on RO desalination systems, powered by renewable energy sources, in the form of digital on/off switching. Some hybrid systems modeling and control work has also been done.[14] A steady state model similar to the one developed in this work can be found in the literature.[11] In addition to these results, there has been recent work by the authors[5] to apply MPC methodologies to an RO desalination system that undergoes feed flow reversal. MPC is implemented to transition optimally from a normal high-flow operating point to a low-flow operating point where it is safe to reverse the flow. Despite these efforts, at this stage there has been no work on model-based control for high recovery RO processes with emphasis on compensation of feedwater variability.

Fault-tolerant control (FTC) structures are based on an underlying assumption that there are more control configurations available than required for the given process.[30,31] The use of the minimum number of control inputs is desirable to minimize unnecessary control action. FTC, in this case, can be achieved through reconfiguration of the control loops in the event of faults. To implement FTC structures on an RO system, first it is necessary to detect and isolate failure events. The results from Mhaskar et al.[25] can be directly applied in order to implement fault detection and isolation (FDI) schemes on an RO system. Other FTC results relevant to this work can be found in the literature.[15,23,24] The authors also have preliminary results on FTC of RO systems to handle actuator faults.[22]

The goal of this work is to develop model-based nonlinear feed-forward/feedback control structures for high recovery RO desalination systems while accounting for such practical issues as sampled and noisy measurements, large time-varying disturbances, and actuator faults. In order to accomplish this goal a detailed mathematical model of a high-recovery RO plant is first developed. This model adequately describes the evolution of process states in time, and it also accounts for the spatial variation of TDS and flow rate inside the membrane units. Most RO models simple enough for control design purposes[16] consider a well mixed model with a single value for concentration on the retentate side of the membrane. However, under high recovery operation the gradients along the length of the membrane unit can be quite significant. As fluid flows axially along the module the bulk concentration increases, the flow rate decreases, and the local permeate flux decreases.[11] The model developed in the present work includes appropriate differential equations in space that account for these gradients. A Lyapunov-based nonlinear controller[10,12] is then applied to this high recovery RO model. One of the main objectives of a controller in high recovery RO is to reject disturbances caused by

* To whom correspondence should be addresseed. E-mail: pdc@seas.ucla.edu.

10.1021/ie071559b CCC: $40.75
Published on Web 07/26/2008

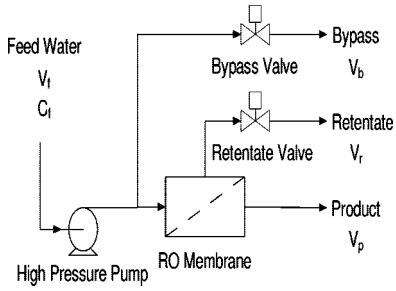

Figure 1. Single-stage high recovery RO membrane desalination process. The two actuated valves, retentate valve and bypass valve, act as manipulated inputs.

feedwater variation. Feed disturbances could cause undesired fluctuations in the product flow rate or the internal pressure. To accomplish disturbance rejection, the control law includes both feedback and feed-forward components (i.e., measurement of feed concentration fluctuations). The feedwater stream concentration can easily be measured in practice, so the first set of simulations presented in this work explore the ability of the proposed control method to reject such disturbances. Another objective is to detect and isolate actuator faults as soon as possible. A second set of simulations demonstrate how FDI and FTC can be applied to this system and how appropriate action can be taken to maintain desired system operation when a fault occurs in the control actuators.

2. Process Description and Modeling

Figure 1 shows a schematic of an elementary RO desalination process. This is a single-stage RO system with no pre-treatment or post-treatment units. Feed brackish water or seawater enters the system through a high pressure pump. This high pressure water then flows across an RO membrane, and low salinity product water permeates through the membrane. Concentrated brine then exits the membrane module and passes through a throttling valve to be discharged at atmospheric pressure. The RO plant consists of a high pressure pump, two automated valves, a spiral wound membrane unit, required plumbing, and tanks. The valve settings can be manipulated in real time based on measurement information which includes the flow velocities and feed concentration.

The first principles model of this system is based on a macroscopic kinetic energy balance, a local mass balance, and a microscopic mass shell balance. This model assumes an incompressible fluid and constant internal volume and mass. It is assumed that the water in the module travels in a plug flow with no back-mixing or axial diffusion. It is also assumed that the osmotic pressure can be related to the TDS at the membrane surface.[21] Skin friction through the piping and the membrane module are considered negligible relative to the hydraulic losses in the throttling valves and across the membrane.

The energy balance consists of two nonlinear ordinary differential equations (ODEs) in time where the velocities of the bypass and retentate stream are the states. Each ODE is derived from an energy balance around an actuated control valve.[6] Specifically, the two ODEs that can describe the process depicted in Figure 1 take the following form:

$$\begin{aligned}\frac{d\upsilon_b}{dt} &= \frac{A_p}{\rho V}\left(P - \frac{1}{2}\upsilon_b{}^2 e_{v1}\right)\\ \frac{d\upsilon_r}{dt} &= \frac{A_p}{\rho V}\left(P - \frac{1}{2}\upsilon_r{}^2 e_{v2}\right)\end{aligned} \tag{1}$$

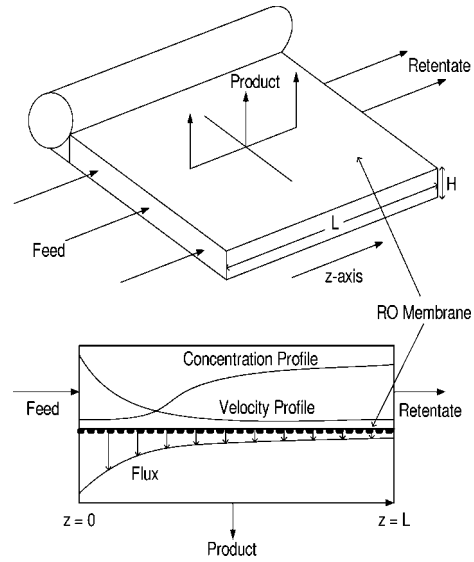

Figure 2. Expanded view of a spiral wound membrane module and typical concentration and velocity profiles inside the module.

where υ_b is the bypass velocity, υ_r is the retentate velocity, A_p is the pipe cross sectional area, V is the total internal volume, ρ is the fluid density, and P is the internal pressure. e_{v1} and e_{v2} are friction loss factors for the actuated valves and act as manipulated inputs. The two ODEs of eq 1 are not explicitly coupled; however, coupling does occur through the pressure term, P. The pressure, P, of the RO system is an algebraic variable which is an implicit nonlinear function of υ_b and υ_r for which there exists no differential equation in time. P is assumed to be space independent throughout the high pressure region by neglecting skin friction. Specifically, P at each time is obtained via solving a local mass balance and a microscopic mass shell balance along the length of the membrane module in space. The local mass balance around the bypass line and feed line junction allows the calculation of the feed velocity to the membrane module, υ_{mf}, given the bypass and retentate velocities from eq 1:

$$\upsilon_f = \upsilon_b + \upsilon_{mf} \tag{2}$$

where υ_f is the constant velocity of the feed stream.

It is critical in a high recovery system, where the concentration and velocity in the module change significantly along the axis of flow, to accurately describe the concentration and velocity profiles along the membrane module. In order to model these profiles a shell balance is performed across the length of the membrane module to generate a two state ODE system in space. To clarify how this model is developed, an expanded view of an unwound spiral-wound membrane module and a drawing depicting typical concentration and velocity profiles in a module can be seen in Figure 2. The internal compartment of the membrane module is simplified to a rectangular space. A steady state shell balance is performed on this space assuming radially well mixed plug flow. This steady state approximation is made under the assumption that disturbances on the system will act on a much slower time scale than the residence time in the membrane unit. The shell balances are based on the conservation of TDS mass and water mass inside the membrane module. The differential volume for the shell balance has the dimensions W by H by δz, where δz is an infinitesimal length in the z direction. W is the membrane width ($W = A_m/L$, A_m is the membrane area and L is the membrane length), and H is the channel height. The derivation assumes that dissolved solids

are completely rejected and that only water permeates the membrane at a flux approximated by $J_w = K_m(P - K_{\Delta\pi}C_z)$, where J_w is the permeate flux, K_m is the overall mass transfer coefficient, $K_{\Delta\pi}$ is a constant that relates C_z to osmotic pressure, and C_z is the concentration along the z-axis in the membrane. The result of the shell balance is the following two coupled ODEs in space and three boundary conditions (owing to the fact that P is an algebraic variable):

$$\begin{gathered}\frac{dC_z}{dz} = \frac{C_z}{v_z}\frac{K_m(P - K_{\Delta\pi}C_z)}{\rho H} \\ \frac{dv_z}{dz} = -\frac{K_m(P - K_{\Delta\pi}C_z)}{\rho H} \\ C_z(z=0) = C_f \\ v_z(z=0) = \alpha v_{mf} \\ v_z(z=L) = \alpha v_r\end{gathered} \tag{3}$$

where z is the direction of flow through the membrane, v_z is the velocity of flow in the membrane along the z-axis, and H is the height of the membrane channel. The boundary conditions arise when eq 3 is coupled with eqs 1 and 2. Equation 3 is solved at each time step as we integrate eq 1 in time. The solution to the ODEs of eq 3 is complicated by the fact that they must satisfy three boundary conditions, two at the inlet, and one at the outlet owing to the fact that P is an unknown algebraic variable. The feed concentration, C_f, represents a boundary condition at $z = 0$ (at the membrane inlet) provided as a time varying parameter. The feed velocity to the module, v_{mf}, provides the velocity boundary condition at $z = 0$. Retentate velocity, v_r, provided from eq 1, is a boundary condition at the membrane outlet, $x = L$, where L is the membrane length in the z direction. The parameter α is the ratio of the pipe cross sectional area to the membrane channel cross sectional area. Pressure is the unknown variable in time that must be adjusted in order to find the solution to eq 3. The solution to eq 3 is found at each time by using a type of shooting method[8] where the system pressure is adjusted until all three boundary conditions are satisfied. This system pressure is then substituted into eq 1 for the next step of integration forward in time.

Remark 1. The model of eqs 1−3 can be expanded in several ways to improve the accuracy at the expense of greater model complexity. The pressure, for example, is taken as constant along the length of the membrane module at a specific time instant. However, in a real system there is a minor pressure loss due to skin friction and the pressure will decrease in the z direction. The model could be expanded to handle this by deriving an ODE that describes dP/dz and including it in eq 3. The same solution algorithm would be used, but a guess value for $P(z = 0)$ should be used in the place of P in step 2. Another improvement to the model would be to use transient PDEs to describe the velocity and concentration profiles. This would effectively remove the steady state approximation in eq 3 and would make the model dynamics more accurate on time scales shorter than the membrane residence time. The model could also be expanded to include the concentration gradient in the y direction (the gradient from the bulk solution to the membrane surface), thus giving a more accurate osmotic pressure and product flux. The osmotic pressure term could also be expanded algebraically to include the effects of temperature. There are also other minor modeling improvements that could be made, but the goal is to obtain a model that is computationally tractable yet accurate enough to synthesize model-based feedback control laws.

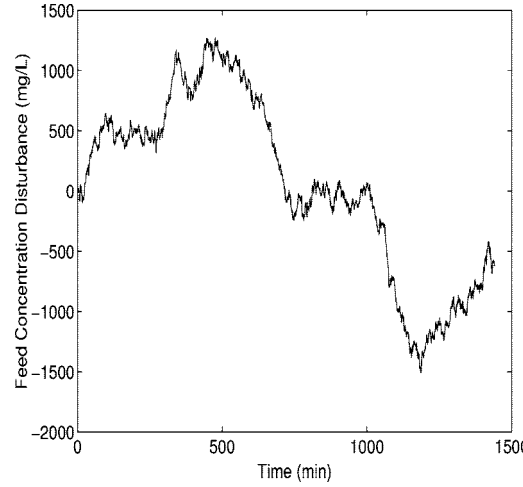

Figure 3. Disturbance on feed concentration versus time, this large time-varying disturbance on the RO system is added to the nominal C_f value.

3. RO Process Model Solution Algorithm

A step-by-step discussion of the algorithm used to compute the solution of the open-loop model of eqs 1–3 is presented to clarify the method employed in this work. An assumption is made that the profiles of C_z and v_z change only with respect to z within each integration step in time; this assumption can be satisfied by picking the time step of integration to be sufficiently small. It is also assumed that C_f changes slowly relative to the residence time in the module which is a reasonable assumption for any real RO process. This allows the independent solution of eq 3 at each time step. A large well-mixed holding tank placed before the feed can act as a low-pass filter to eliminate fast time-scale disturbances.

In order to solve the system of equations presented in eqs 1–3 numerically, the following algorithm is applied.

1. Initial conditions for v_b and v_r are chosen.
2. v_{mf} is computed from eq 2.
3. Given v_{mf}, C_f, and a guess value for P, a solution to eq 3 is computed numerically.
4. The resulting $v_z(z = L)$ is compared to αv_r, and P is adjusted via shooting method until $v_z(z = L)$ is equal to αv_r.
5. The value of P resulting from step 4 is used in eq 1 to integrate numerically one step forward in time.
6. The results of step 5 provide updated values of the states, v_b and v_r, and the algorithm returns to step 1 using these values as new initial conditions. This process is repeated until the desired integration time is reached.

The open-loop simulation results can be seen as the solid lines in Figures 4–7 for the parameters in Table 1. The simulation is run at high recovery (just over 90% recovery) for a time of 24 h with a time varying disturbance on C_f as defined in Figure 3. This disturbance was generated from sinusoidal functions and autocorrelated noise to give an approximation of disturbances encountered in practice. It can be seen that v_b and v_p oscillate due to the disturbance, but the oscillations are not large relative to the steady state values for these states. However, Figure 6 shows wide swings in the internal pressure for the open-loop case. This type of behavior could lead to safety issues if the pressure exceeds the safety rating of hoses, fittings, or

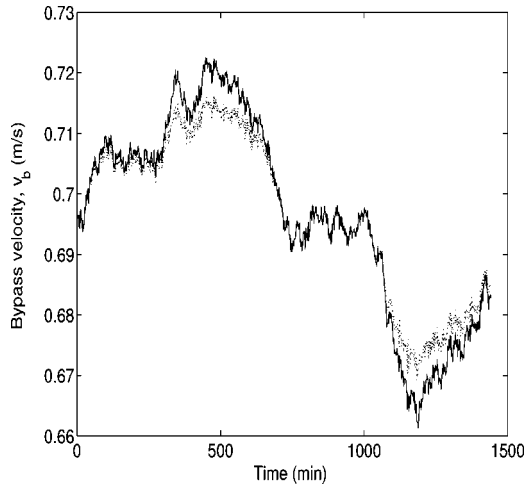

Figure 4. Bypass velocity, v_b, profiles versus time; open-loop (solid line), closed-loop feedback control without disturbance measurements (dotted line).

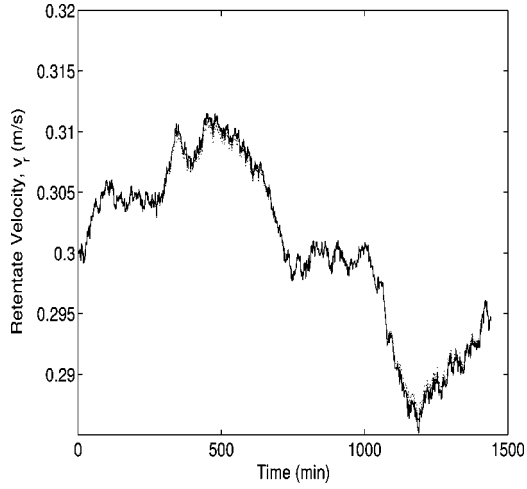

Figure 5. Retentate velocity, v_r, profiles versus time; open-loop (solid line), closed-loop feedback control without disturbance measurements (dotted line). The dotted line nearly overlaps the solid line.

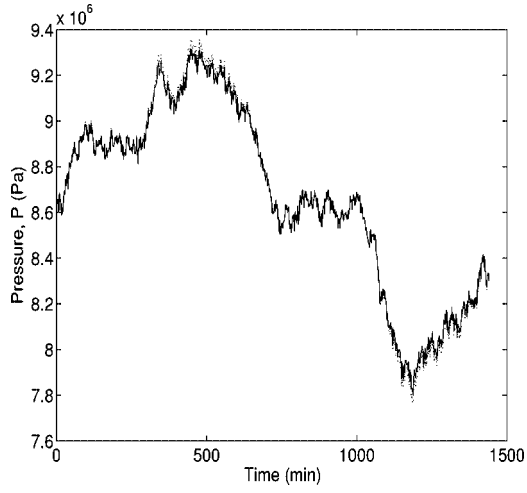

Figure 6. Internal pressure, P, profiles versus time; open-loop (solid line), closed-loop feedback control without disturbance measurements (dotted line). The dotted line nearly overlaps the solid line.

pressure vessels. This motivates the use of feedback control to reduce the effects of feed disturbances on the process.

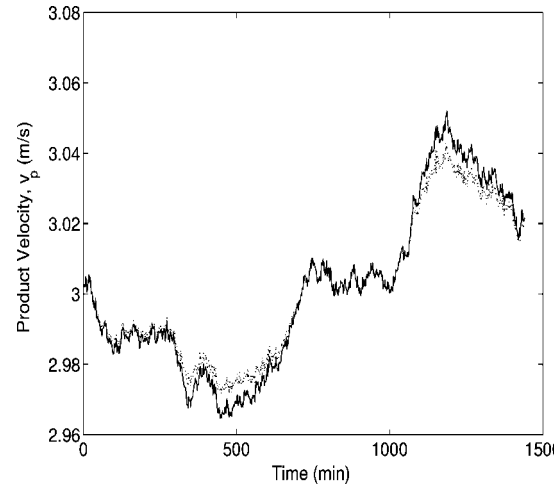

Figure 7. Product velocity, v_p, profiles versus time; open-loop (solid line), closed-loop feedback control without disturbance measurements (dotted line).

Table 1. Process Parameters and Steady State Values

$\rho = 1000$	kg/m^3
$V = 0.1$	m^3
$v_f = 4.0$	m/s
$A_p = 1.27$	cm^2
$A_m = 13$	m^2
$K_m = 9.218 \times 10^{-9}$	s/m
$K_{\Delta\pi} = 78.7$	Pa/(mg/L)
$C_f = 10000$	mg/L
$H = 1.0$	mm
$L = 5.0$	m
$\alpha = 0.049$	
$C_f^{ss} = 10000$	mg/L
$e_{v1}^{ss} = 3.57 \times 10^7$	
$e_{v2}^{ss} = 1.92 \times 10^8$	
$v_b^{ss} = 0.7$	m/s
$v_r^{ss} = 0.3$	m/s
$v_p^{ss} = 3.0$	m/s
$P^{ss} = 8.61 \times 10^6$	Pa

4. Feedback Controller Synthesis

The potential manipulated inputs to the system are the friction loss factors for the valves (e_{v1} and e_{v2}). Valves can be manipulated in practice by an automated electric motor that partially opens or closes the valves. The measured outputs are the bypass velocity (v_b), retentate velocity (v_r), and internal pressure (P). The superscript ss corresponds to the high recovery steady state values for this system when $C_f^{ss} = 10\,000$ mg/L, corresponding to a brackish feedwater source. Operation at this point provides a recovery of 91%.

One control objective is to stabilize the process at the desired retentate velocity, v_r, and operating pressure, P, in the presence of large time varying disturbances in the feed concentration C_f. This configuration would be used on a system that operates close to the maximum allowable internal pressure. The internal pressure often needs to be below a specified value for safety reasons (safety ratings for fittings and pressure vessels), and at high recovery an RO plant may operate close to this safety threshold. Another control objective could be to stabilize the process at the desired retentate velocity, v_r, and the desired product flow rate, v_p. This type of disturbance rejection may be used on RO systems that are designed for extremely high pressures and allows for a consistent delivery of product water. The controller will use both e_{v1} and e_{v2} as manipulated inputs.

To present the controller design method in a concise form, the model of eq 1 is written in a deviation variable form around

the desired steady state. The states are defined as $x = [x_1 x_2]^T$ where $x_1 = \upsilon_b - \upsilon_b^{ss}$ and $x_2 = \upsilon_r - \upsilon_r^{ss}$. The plant can then be described by the following nonlinear continuous-time ODE system:

$$\dot{x}(t) = f(x(t)) + g(x(t))\,u(t) + w(x(t))\,d(t)$$
$$|u_i| \le u_i^{\max} \tag{4}$$

where $x(t) \in \boldsymbol{R}^2$ denotes the vector of process state variables, $u(t)$ is a vector of inputs where $u(t) = [u_1\ u_2]^T$ $u_i(t) \in [-u_i^{\max}, u_i^{\max}] \subset \boldsymbol{R}$ denotes the ith constrained manipulated input, $u_1(t) = e_{v1} - e_{v1}^{ss}$ and $u_2(t) = e_{v2} - e_{v2}^{ss}$, and $d(t)$ denotes the disturbance on the system, $d(t) = P - P^{ss}$. The disturbance in this system originates from the feed concentration, C_f, but $d(t)$ is expressed in terms of P because C_f acts on P in an algebraic fashion through eq 3. The control objective is to maintain the outputs at their desired values in the presence of large time varying disturbances on the feed concentration. The state feedback control problem where measurements of all process states are available for all times is considered because velocities, υ_b and υ_r, can be readily measured in practice. The disturbance, $d(t)$, is available as a measurement of C_f, and C_f can be used to calculate P and, hence, $d(t)$. Since $d(t)$ is readily available, $\hat{f}(x(t)) = f(x(t)) + w(x(t))d(t)$ is defined.

Next, a Lyapunov-based nonlinear feedback controller that enforces asymptotic stability in the presence of actuator constraints is synthesized. First, a quadratic Lyapunov function of the form $V_L = x^T P_L x$ is defined where P_L is a positive-definite symmetric matrix. This Lyapunov function is used to synthesize a bounded nonlinear feedback control law[10,13,19] of the form

$$u_k = -r(x, u^{\max}) L_g V_L \tag{5}$$

where

$$r = \frac{L_f^* V_L + \sqrt{(L_f^* V_L)^2 + (u^{\max}|L_g V_L|)^4}}{(|L_g V_L|)^2\left(1 + \sqrt{(u^{\max}|L_g V_L|)^2}\right)} \tag{6}$$

and $L_f^* V_L = L_f V_L + \alpha V_L$, $\alpha > 0$. The scalar function $r(\cdot)$ in eqs 5 and 6 can be considered as a nonlinear controller gain.

If the value of $d(t)$ is available at each time the Lyapunov-based feedback controller of eqs 5 and 6 employs a feed-forward compensation component. In this case the controller is updated with the latest disturbance information to reject the effects of the disturbance on the states, υ_b and υ_r. In practice it is possible to use a conductivity meter in the feed line to get real-time measurements of the disturbance. However, if the value of $d(t)$ is not available for measurement at each time, $P = P^{ss}$ for the control law and the controller acts in a standard Lyapunov-based feedback manner using a nominal value for $d(t)$. In this case, control action is not taken until the states have moved away from the steady state values due to the disturbance, and the control action does not completely compensate for the disturbance.

5. FDI and FTC

In addition to feedback control and disturbance compensation, the problem of actuator FDI and FTC is also addressed. Given the properties of the dynamic model of eqs 1–3, it can be shown that the primary control configuration with e_{v1} and e_{v2} as manipulated inputs satisfies the requirements of achieving FDI of actuator faults (see Mhaskar et al.[25] for details). This section presents the methods used to implement fault detection and isolation and fault-tolerant control (FDIFTC) on this high recovery RO process. First, the existence of fall-back control configurations is discussed. Next, the construction and explicit forms of FDI filters for the primary configuration are presented. Finally, a switching law that orchestrates the reconfiguration of the control system in a way that provides closed-loop stability in the event of actuator failures is presented.

5.1. Fall-Back Control Configurations. In order to carry out FTC there must be some redundant control inputs that can be used to control the system in the event of a failure. For this RO system let the initial control configuration, $k(t = 0) = 1$, be the primary configuration with e_{v1} and e_{v2} as manipulated inputs. For the first fall-back configuration consider the system shown in Figure 1 with an identical fall-back actuator for the retentate valve, e_{v2}^{fb}. Flow can be diverted from the primary retentate valve (e_{v2}) to the fall-back retentate valve (e_{v2}^{fb}) through the use of simple on/off valves. Let $k = 2$ be this fall-back configuration with e_{v1} and e_{v2}^{fb} as manipulated inputs. For the second fall-back configuration consider the RO system with an additional fall-back valve for the bypass. Let $k = 3$ be the fall-back configuration with e_{v1}^{fb} and e_{v2} as the manipulated inputs.

5.2. FDI Filters. The FDI filters should enable the detection and isolation of an actuator fault by observing the behavior of the closed-loop process. This is done by using real-time measurements of system states to decouple the ODEs in time. The FDI filter design for the primary control configuration takes the form

$$\frac{d\tilde{\upsilon}_b}{dt} = \frac{A_p}{\rho V}\left(\tilde{P}_1 - \frac{1}{2}\tilde{\upsilon}_b^2 e_{v1}\right), \quad \tilde{\upsilon}_b(0) = \upsilon_b(0)$$
$$\frac{d\tilde{\upsilon}_r}{dt} = \frac{A_p}{\rho V}\left(\tilde{P}_2 - \frac{1}{2}\tilde{\upsilon}_r^2 e_{v2}\right), \quad \tilde{\upsilon}_r(0) = \upsilon_r(0) \tag{7}$$
$$r_b = |\upsilon_b - \tilde{\upsilon}_b|$$
$$r_r = |\upsilon_r - \tilde{\upsilon}_r|$$

where $\tilde{\upsilon}_b$ and $\tilde{\upsilon}_r$ are the FDI filter states for the bypass and retentate velocity, respectively. r_b is the residual associated with the bypass valve, and r_r is the residual associated with the retentate valve. $\tilde{P}_1$ is a function of $\tilde{\upsilon}_b$ and υ_r. $\tilde{P}_2$ is a function of υ_b and $\tilde{\upsilon}_r$. $\tilde{P}_1$ and $\tilde{P}_2$ are calculated for each time using the above algorithm and eqs 2 and 3 with the appropriate values for υ_b, υ_r, $\tilde{\upsilon}_b$, and/or $\tilde{\upsilon}_r$. The filter states are initialized at the same value as the process states ($\tilde{\upsilon}(0) = \upsilon(0)$) and essentially predict the evolution of the process in the absence of actuator faults. The residual associated with each manipulated input captures the difference between the predicted evolution of the states in the absence of a fault on that actuator and the evolution of the measured process state. If a given residual becomes nonzero, a fault is declared on the associated input. For a detailed mathematical analysis of the FDI properties of the filter, the reader may refer to Mhaskar et al.[25]

5.3. Fault-Tolerant Supervisory Switching Logic. The next step is to design a switching logic that the plant supervisor will use to decide what fall-back control configuration to implement given an actuator failure. The supervisor should only implement those configurations that do not utilize a failed actuator. Let T_{fault} be the time of an actuator failure, and T_{detect} be the earliest time at which the value of $r_i(t) > \delta r_i > 0$ (for the ith input where δr_i is the ith detection threshold). The switching rule given by

$$k(t \ge T_{detect}) = 2 \quad \text{if} \quad r_r(t) > \delta r_r$$
$$k(t \ge T_{detect}) = 3 \quad \text{if} \quad r_b(t) > \delta r_b \tag{8}$$

guarantees asymptotic closed-loop stability if the new configuration does not include any faulty actuators. The switching law requires monitoring of FDI filters and activation of a fall-back control configuration when a threshold is exceeded.

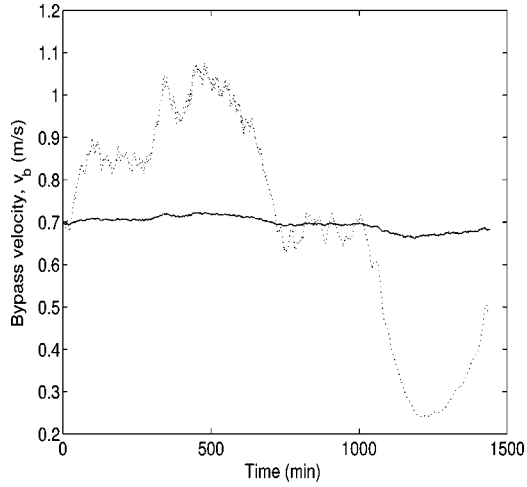

Figure 8. Bypass velocity, v_b, profiles versus time; open-loop (solid line) and under PI control with P and v_r as controlled outputs (dotted line).

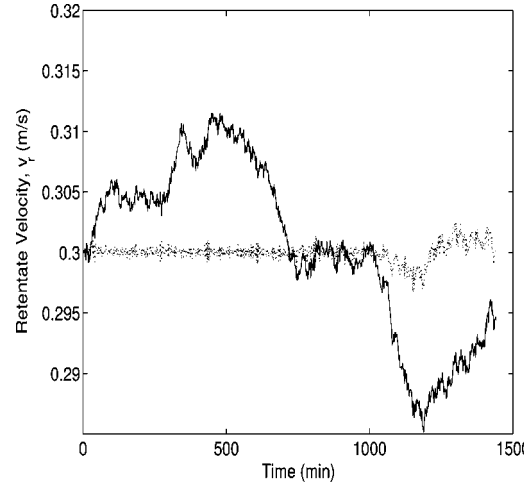

Figure 9. Retentate velocity, v_r, profiles versus time; open-loop (solid line) and under PI control with P and v_r as controlled outputs (dotted line).

Remark 2. In general when considering FDI and FTC for a nonlinear system using the framework proposed in Mhaskar et al.[25] one needs to account for the stability region of each bounded control configuration and switch only to a control configuration that guarantees stability. However, in the case of an RO system, stability is not the focus because the system is inherently very stable even when operated open-loop and converges quickly to the steady state equilibrium point. Therefore, the main goal of feedback control in the RO application is not to enforce stability on the system but to improve performance and handle events such as actuator faults and feed disturbances.

6. Simulation results

The simulation results section is divided into two subsections where the first subsection considers a large time-varying disturbance on the feed concentration, as shown in Figure 3, and the second subsection considers actuator failures in addition to this disturbance. Time varying disturbances in the feed concentration tend to occur on a long time scale (hours or days); however, failures in the actuators are often sudden and propagate quickly (on the order of 1 s or less).

6.1. Large Time Varying Disturbance. This section considers the application of three different nonlinear control algorithms to handle a large time-varying disturbance in the feed concentration, C_f. Proportional/integral (PI) control is also implemented on the system as a point of comparison.

6.1.1. PI Feedback Control: P and v_r as the Controlled Outputs. The first simulation scenario involves using two PI loops to handle the time varying disturbance on the feed concentration, as shown in Figure 3. The first PI loop uses the bypass valve to control the value of the term P. For the first loop the measurement is P, and the manipulated input is e_{v1}. The second PI loop uses the retentate valve to control the state v_r. For the second loop the measurement is v_r and the manipulated input is e_{v2}. The proportional gain, K, and the integral time, τ_I, could not be tuned using standard tuning methods as in[26,28] because of nonlinearities and the coarse grained sampling time. For this reason, the gains and integral time constants were determined through trial and error runs. The system has a sampling time of 60 s, and the controller implementation is sample and hold. The results can be seen in Figures 8–12. While PI control is able to reject the disturbance under some conditions, it ultimately fails to keep P and v_r at the desired values due to the time varying nature of the disturbance.

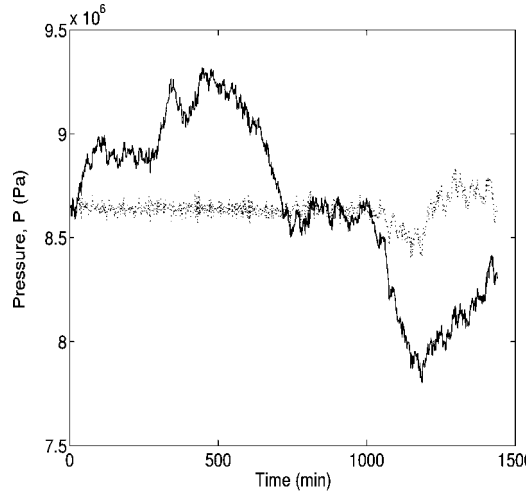

Figure 10. Internal pressure, P, profiles versus time; open-loop (solid line) and under PI control with P and v_r as controlled outputs (dotted line).

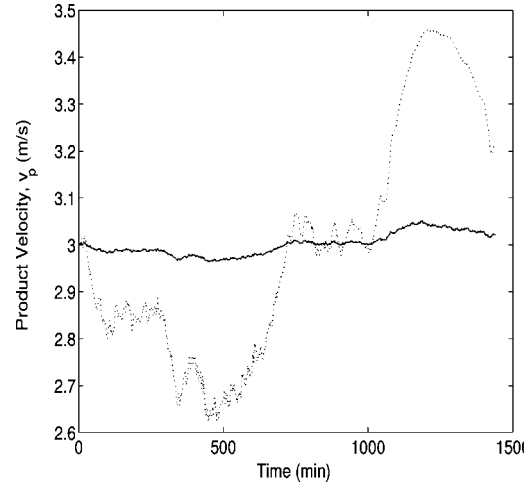

Figure 11. Product velocity, v_p, profiles versus time; open-loop (solid line) and under PI control with P and v_r as controlled outputs (dotted line).

6.1.2. Feedback Control: v_b and v_r are the Controlled Outputs. This simulation scenario involves using the Lyapunov-based control law presented in eq 5. This scenario considers

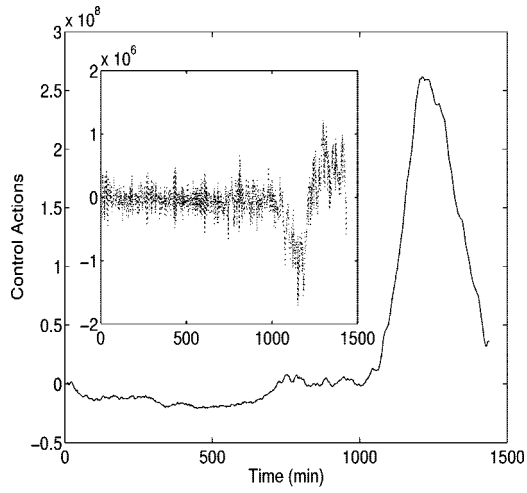

Figure 12. Manipulated inputs for the PI controller with P and υ_r as the controlled outputs. Control action applied to e_{v1} and e_{v2} are the solid and dotted lines, respectively.

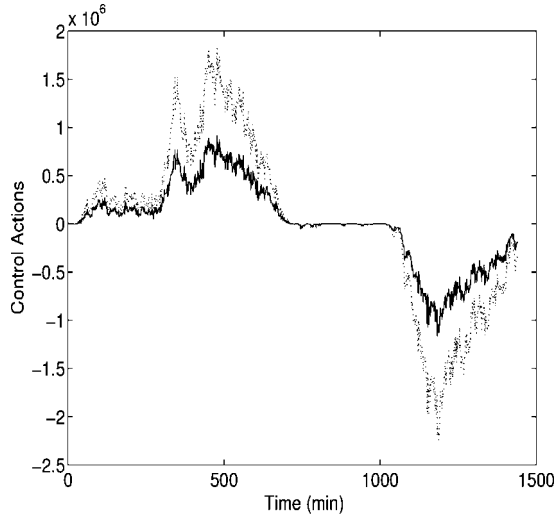

Figure 13. Manipulated inputs for the Lyapunov-based feedback controller with no feed-forward compensation with υ_b and υ_r as the controlled outputs. Control actions applied to e_{v1} and e_{v2} are the solid and dotted lines, respectively.

the same dynamic disturbance as in the previous case, where C_f varies with time according to Figure 3. The states, υ_b and υ_r, are sampled at a rate of one measurement per 60 s which is well within the capabilities of existing sensing systems. The control action for the manipulated inputs is computed once per 60 s based on these measurements. This control action is implemented for the duration of the sample time, which is 60 s, in a sample-and-hold fashion. The disturbance is not measured in this case. The value of P used in $\hat{f}(x(t))$ is P^{ss} for all t, and the controller does not compensate well for the disturbance on C_f.

The closed-loop simulation results can be seen as the dotted lines in Figures 4–7. The manipulated inputs can be seen in Figure 13. The states, υ_b and υ_r, and the product flow, υ_p, oscillate at a marginally lower magnitude than the corresponding profiles for the open-loop case, so the feedback control is able to slightly damp out the effects of the disturbance. If the gain of the controller is increased by changing P_L, it is possible to decrease the disturbance effect further at the expense of higher control actions and possible instability at this sampling rate. However, the pressure oscillates at a somewhat higher magnitude than in the open-loop simulation, and this may not be acceptable for safety reasons. This type of feedback control may be useful for the case where regulating the states and product flow rate is more important than regulating the internal pressure, for example, when the system is being operated at a pressure far below its rated maximum. However, the poor performance of feedback alone motivates the addition of feed-forward compensation to the controller that takes advantage of C_f measurements.

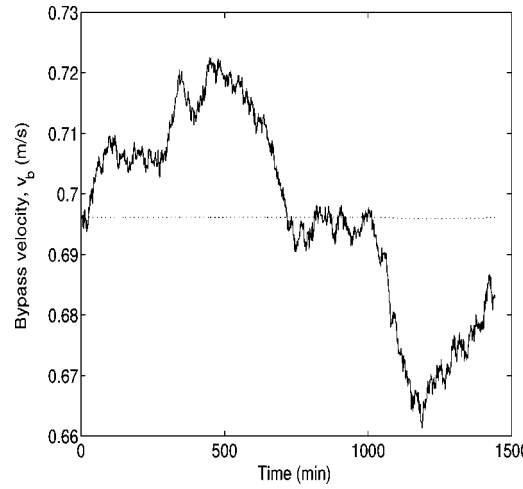

Figure 14. Bypass velocity, υ_b, profiles versus time; open-loop (solid line) and under feed-forward/feedback control with υ_b and υ_r as controlled outputs (dotted line).

6.1.3. Feed-Forward/Feedback Control: υ_b and υ_r are the Controlled Outputs. The second simulation scenario involves using the Lyapunov-based control law presented in eq 5, with model-based feed-forward compensation. This technique takes advantage of the dynamic model and the ability to measure C_f to produce better closed-loop system performance. For this scenario the time varying nature of C_f is the same as in the open-loop case. Measurements of the states and of the disturbance, C_f, are sampled at a rate of one per 60 s. At each sampling time a control action is computed and implemented in a sample-and-hold fashion. At each sampling time eqs 1–3 are solved for the parameters contained in $\hat{f}(x(t))$ corresponding to the current C_f value and the desired υ_p and υ_r values. This can be done with the following steps:

1. Choose set points for υ_b and υ_r, in this case 0.7 and 0.3 m/s, respectively, to achieve a recovery of over 90%.
2. Solve eq 2) for υ_{mf}.
3. Find the appropriate P, via shooting method, to satisfy all the boundary conditions for eq 3.
4. Set eq 1 equal to zero and solve for e_{v1}^{nom} and e_{v2}^{nom}. These are the nominal values for the manipulated inputs that will compensate for the current disturbance, $C_f(t)$, and are components of $\hat{f}(x(t))$.

The control law in eq 5 is used to compute a feedback control action based on the current $\hat{f}(x(t))$ obtained from the above algorithm. This control action is added to the nominal e_{v1}^{nom} and e_{v2}^{nom} values and implemented on the valves. This process is repeated at each sampling time to obtain a feedback control action that includes feed-forward compensation. The manipulated inputs can be seen in Figure 18, and compared to Figure 13 the control actions are larger, yet they are within reasonable actuator limits.

The simulation results can be seen as the dotted lines in Figures 14–17. The values of υ_b, υ_r, and υ_p all stay very close to the steady state values given in Table 1, and the effects of the disturbance are effectively damped. A shorter sampling

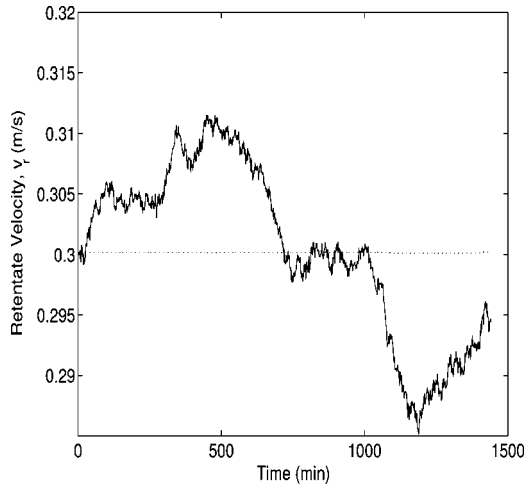

Figure 15. Retentate velocity, v_r, profiles versus time; open-loop (solid line) and under feed-forward/feedback control with v_b and v_r as controlled outputs (dotted line).

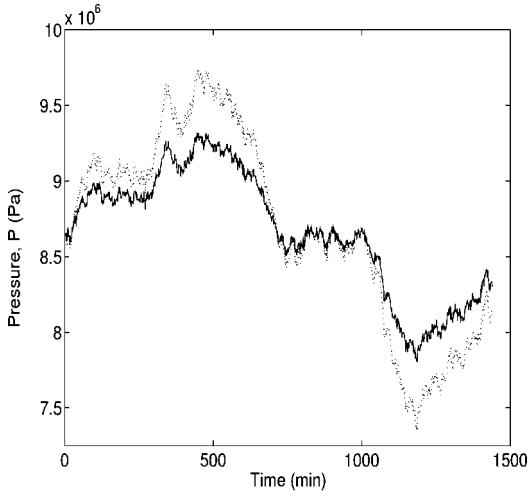

Figure 16. Internal pressure, P, profiles versus time; open-loop (solid line) and under feed-forward/feedback control with v_b and v_r as controlled outputs (dotted line).

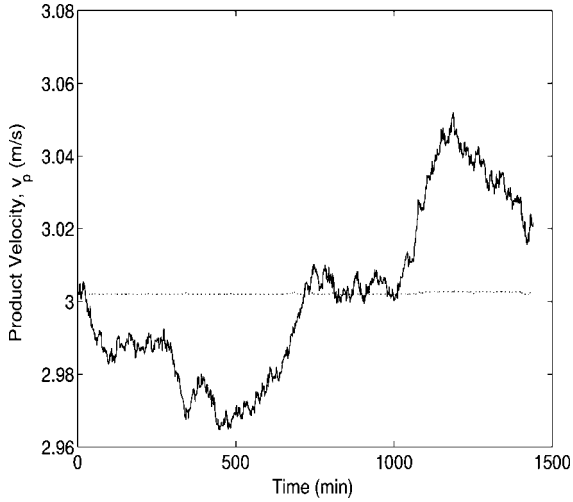

Figure 17. Product velocity, v_p, profiles versus time; open-loop (solid line) and under feed-forward/feedback control with v_b and v_r as controlled outputs (dotted line).

interval would reduce the disturbance effects even further. In this case, the value of P swings sharply in order to compensate for the changing feed conditions. To achieve the desired recovery of over 90% even when the $C_f(t)$ is much higher than C_f^{ss} requires very high pressures. This type of control would be advantageous only when product flow rate is a critical parameter that cannot be disturbed, and the RO system is designed to handle such high internal pressures.

6.1.4. Feed-Forward/Feedback Control: P and v_r are the Controlled Outputs. The third simulation scenario does not fall directly under the Lyapunov-based feed-forward/feedback framework utilized in the previous two simulations; however, it is an important one from a practical point of view. For safety reasons, the large internal pressures exemplified in the previous examples motivate the use of feed-forward/feedback control that maintains $P(t)$ at a constant value, P^{ss}. In order to accomplish this, another variable (either v_b or v_r) must be used to compensate for the effects of C_f. The flow rate v_r is often constrained due to the membrane module capacity, so v_b is an excellent candidate for this role. The bypass velocity can vary widely with little to no ill-effect on the system: v_b is readily recycled, there are usually no downstream lines that depend on v_b, and there are no dominant safety issues associated with wide v_b variations.

The third simulation scenario involves using a Lyapunov-based nonlinear feedback control law similar to the one presented in eq 5. Again, C_f is the same as the previous scenarios, and measurements of the states and disturbance are obtained at a rate of one sample per 60 s. The control action is implemented in a sample-and-hold fashion.

The framework for the feedback control with feed-forward compensation with P and v_r as the controlled outputs is slightly different than the one used in the previous two examples. Specifically, at each sampling time eqs 1–3 are solved for the steady state corresponding to the current C_f value and the desired P and v_r values. This can be done with the following steps:

1. Choose set points for P and v_r, in this case 8.6×10^6 Pa and 0.3 m/s, respectively.

2. Solve eq 3) with the following two boundary conditions using shooting method where an initial guess is made on $v_z(z = 0)$:

$$C_z(z = 0) = C_f \quad \text{(a)}$$

$$v_z(z = L) = \alpha v_r \quad \text{(b)}$$

3. The resulting value of $v_z(z = 0)$ from the previous step is used to calculate v_{mf}.

4. v_{mf} is used with eq 2 to calculate a desired value for v_b. This v_b and the set point for v_r designate a new desired operating point where $P(t) = P^{ss}$.

5. Set eq 1 equal to zero, substitute in the values for P, v_r, and v_b, and solve for e_{v1}^{nom} and e_{v2}^{nom}.

The control law in eq 5 is then used to compute a control action based on this new operating point provided from the above algorithm. This control action is added to the e_{v1}^{nom} and e_{v2}^{nom} values from the above algorithm and implemented on the valves. This process is repeated at each sample time to obtain a new operating point and compute a control action that has feed-forward and feedback components. In other words, at each sampling time the steady state problem of eqs 1–3 is solved to find the desired operating point where $P(t) = P^{ss}$ and $v_r(t) = v_r^{ss}$, and a control action from a Lyapunov-based control law is implemented based on this new operating point. The manipulated input profiles resulting from this control algorithm, e_{v1} and e_{v2}, are shown in Figure 23.

The closed-loop feed-forward/feedback control with P and v_r as controlled outputs can be seen as the dotted line in Figures

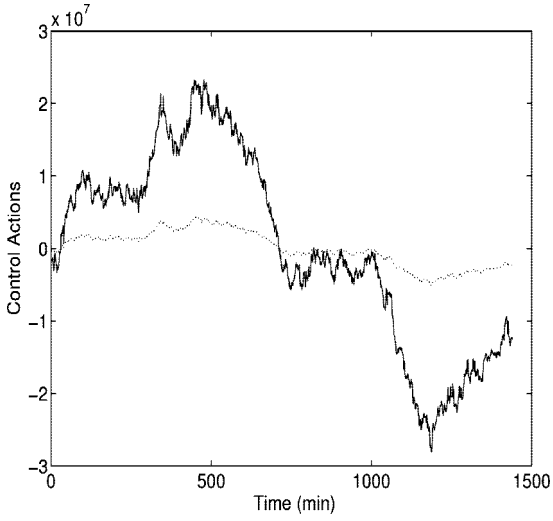

Figure 18. Manipulated inputs for the feed-forward/feedback controller with υ_b and υ_r as the controlled outputs. Control actions applied to e_{v1} and e_{v2} are the solid and dotted lines, respectively.

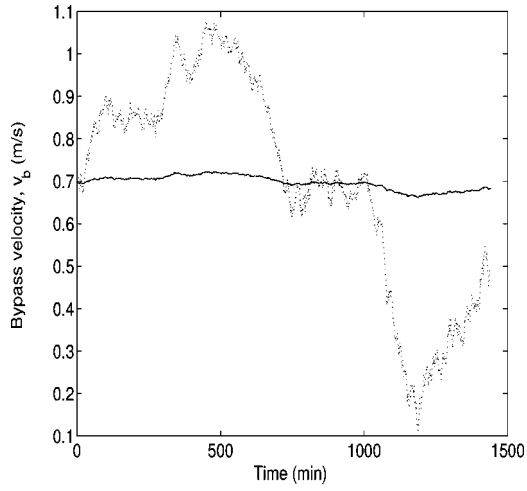

Figure 19. Bypass velocity, υ_b, profiles versus time; open-loop (solid line) and under feed-forward/feedback control with P and υ_r as controlled outputs (dotted line).

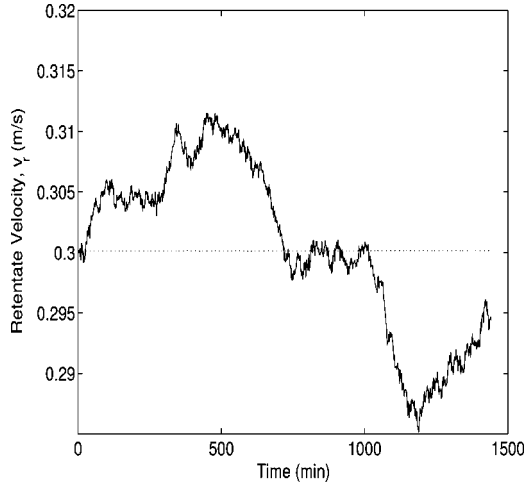

Figure 20. Retentate velocity, υ_r, profiles versus time; open-loop (solid line) and under feed-forward/feedback control with P and υ_r as controlled outputs (dotted line).

19–22. In this case, the pressure, P, stays close to the desired set point, and the effects of the disturbance on pressure and

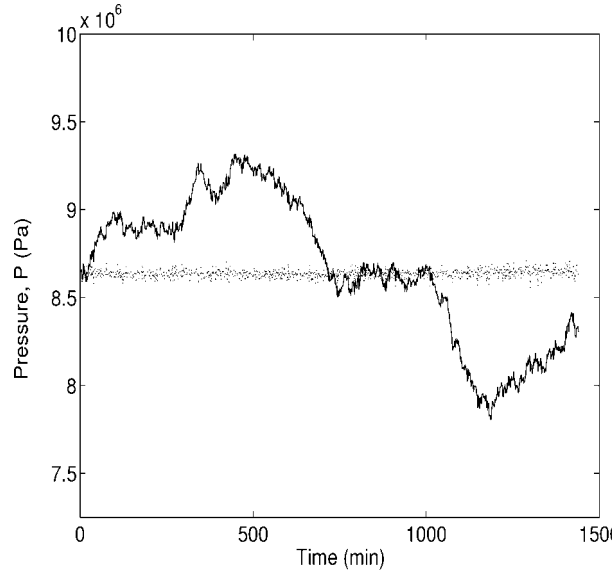

Figure 21. Internal pressure, P, profiles versus time; open-loop (solid line) and under feed-forward/feedback control with P and υ_r as controlled outputs (dotted line).

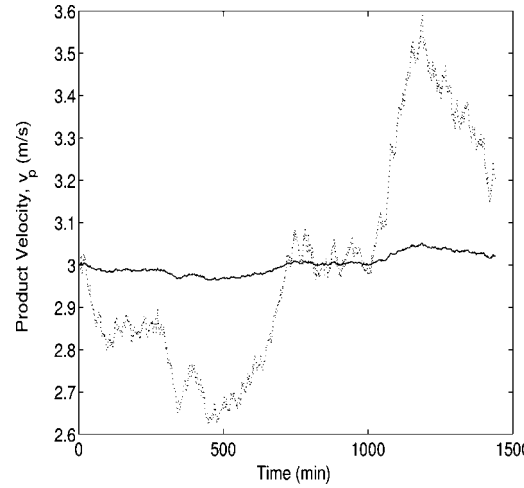

Figure 22. Product velocity, υ_p, profiles versus time; open-loop (solid line) and under feed-forward/feedback control with P and υ_r as controlled outputs (dotted line).

retentate velocity are largely damped. To maintain this pressure, however, the bypass velocity, υ_b, now varies to a large degree to act as a buffer and absorb the effects of the feed disturbance. The manipulated input e_{v1} also varies to accomplish this control task. This type of feed-forward/feedback control is the best to use in a situation where the plant is operating close to the high pressure constraints, which is usually the case at very high recoveries. This type of control is desirable because the bypass velocity can vary widely with little to no ill effects on the system: υ_b is readily recycled, there are usually no downstream structures that depend on υ_b, and there are no major safety issues associated with wide υ_b variations.

Remark 3. Energy efficiency is often a critical concern in the operation of RO plants to minimize environmental and economic costs. Inherently, a bypass line without an energy recovery device is an energy waster because pressurized feedwater is throttled, and energy is lost to friction. It is possible to operate an RO system under a feed-forward/feedback framework as described above using a variable frequency drive (VFD) on the pump. In this case, the control system could

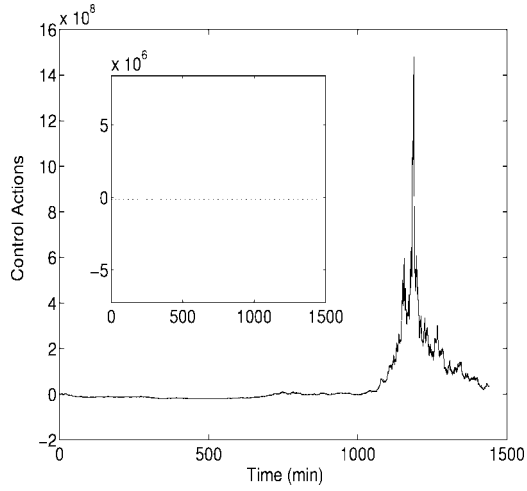

Figure 23. Manipulated inputs for the feed-forward/feedback controller with P and v_r as the controlled outputs. Control actions applied to e_{v1} and e_{v2} are the solid and dotted lines, respectively.

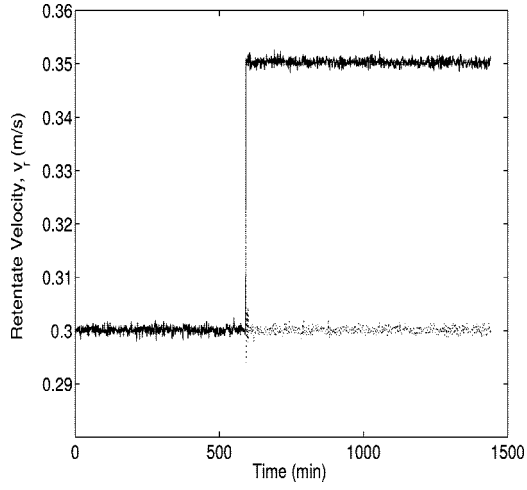

Figure 24. Retentate velocity, v_r, profile versus time; subject to a failure in e_{v2} (solid line) and with FDIFTC recovery (dotted line).

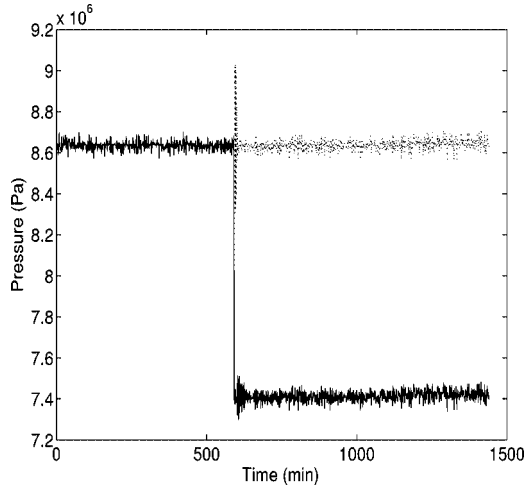

Figure 25. System pressure, P, profile versus time; subject to a failure in e_{v2} (solid line) and with FDIFTC recovery (dotted line).

regulate the VFD and pump speed in order to change system pressure and flow rather than wasting energy by sending pressurized water through a bypass line. For example, if a VFD was used, v_f could be considered as a manipulated input, and

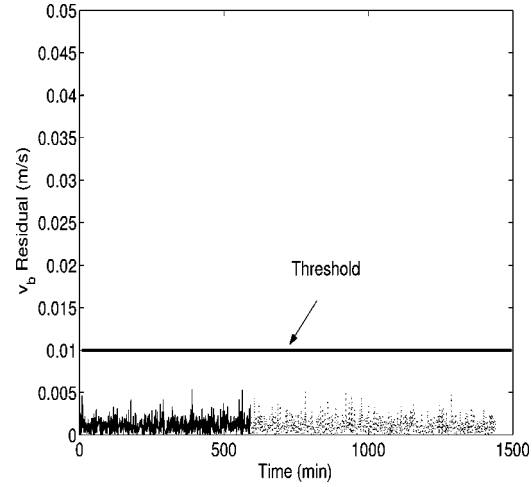

Figure 26. Residual corresponding to the bypass valve versus time. No fault is detected on the bypass valve. The solid line is under the primary control configuration, and the dotted line is under the fall-back configuration.

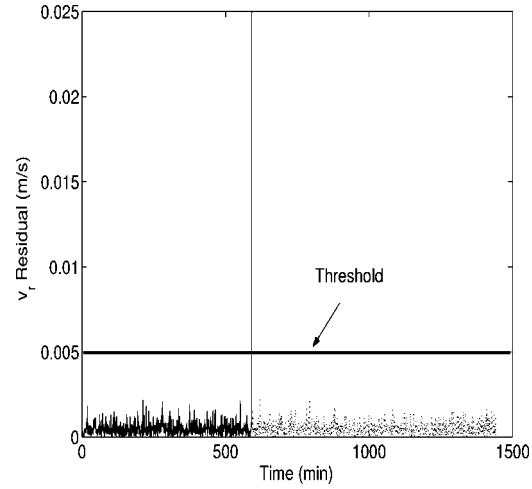

Figure 27. Residual corresponding to the retentate valve versus time. A fault is detected in this valve at $t = 592$ min. The solid line is under the primary control configuration, and the dotted line is under the fall-back configuration.

v_b could be removed from the system. For safety reasons, however, emergency bypass lines that open at a high pressure threshold should still be installed to prevent the accidental overpressurization of the system.

6.2. Actuator Failures. This section considers the application of FDI and FTC to handle valve actuator failures. This plant model is the same as the system used in the previous example with the same time varying disturbance on the feed concentration. Additionally the system is considered to have noisy sampled measurements. The retentate velocity measurements are subject to Gaussian noise with a standard deviation of 6×10^{-4} m/s, and the bypass velocity measurements are subject to Gaussian noise with standard deviation of 1.4×10^{-3} m/s. The standard deviation of the noise is 0.2% of the nominal flow values. In order to isolate a failure, the sampling time must be much faster than the system dynamics. If the sampling time is too slow, then a failure occurring between sampling times will propagate to all system states, and the FDI filter will not function properly. An adequate sampling time can be estimated by examining the open-loop response time of the system. The sampling time must be significantly shorter than the response

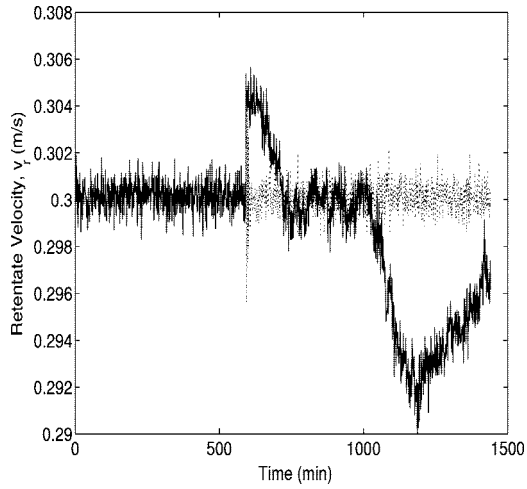

Figure 28. Retentate velocity, v_r, profile versus time; subject to a failure in e_{v1} (solid line) and with FDIFTC recovery (dotted line).

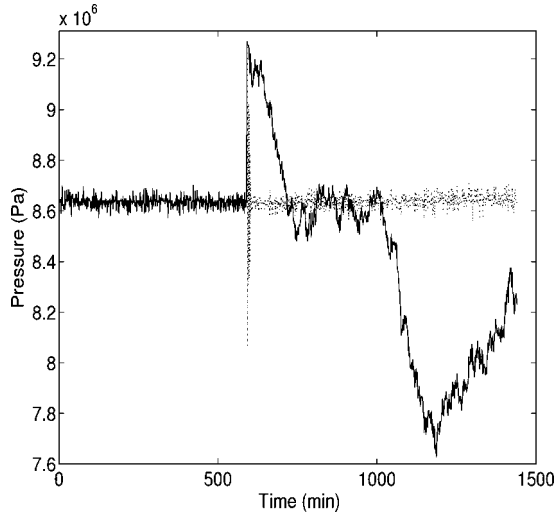

Figure 29. System pressure, P, profile versus time; subject to a failure in e_{v1} (solid line) and with FDIFTC recovery (dotted line).

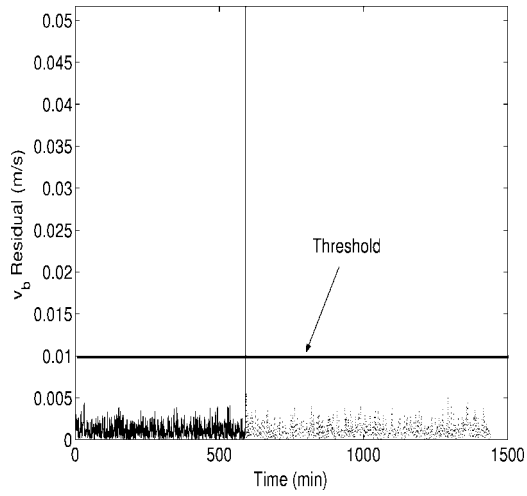

Figure 30. Residual corresponding to the bypass valve versus time. A fault is detected in this valve at $t = 592$ min. The solid line is under the primary control configuration, and the dotted line is under the fall-back configuration.

time. This is practically possible given that the filter only requires measurements of v_b and v_r. Furthermore, while the FDI component requires a fast sampling rate in order to do isolation,

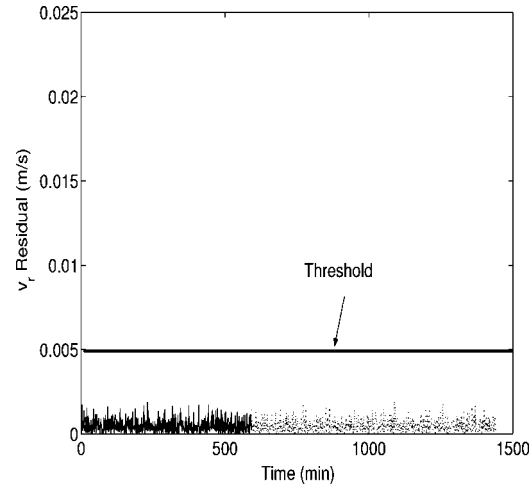

Figure 31. Residual corresponding to the retentate valve versus time. No fault is detected on the retentate valve. The solid line is under the primary control configuration, and the dotted line is under the fall-back configuration.

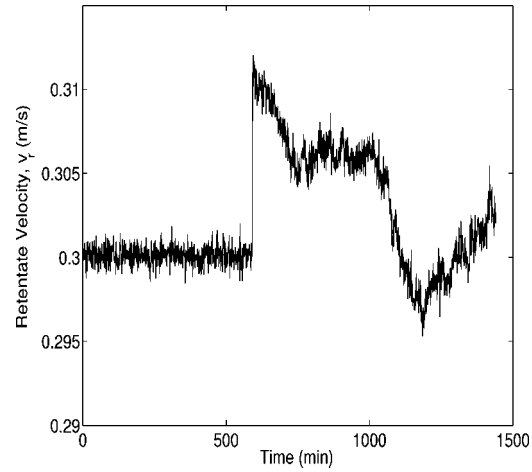

Figure 32. Retentate velocity, v_r, profile versus time; subject to a failure in e_{v1}.

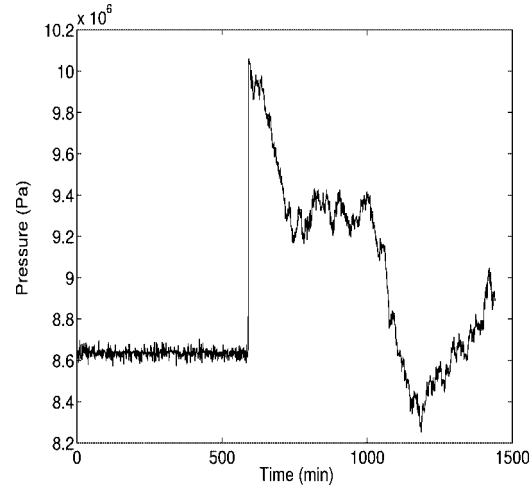

Figure 33. System pressure, P, profile versus time; subject to a failure in e_{v1}.

the FTC reconfiguration can happen on a much slower time scale. FTC reconfiguration could be delayed for several moments after a fault is isolated; however, the states may move to an undesired region during this delay. This is clearly better than

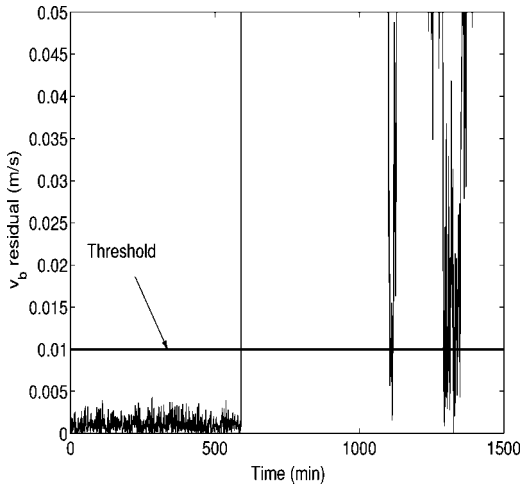

Figure 34. Residual corresponding to the bypass valve versus time. The residual is exceeded at $t = 592$ min.

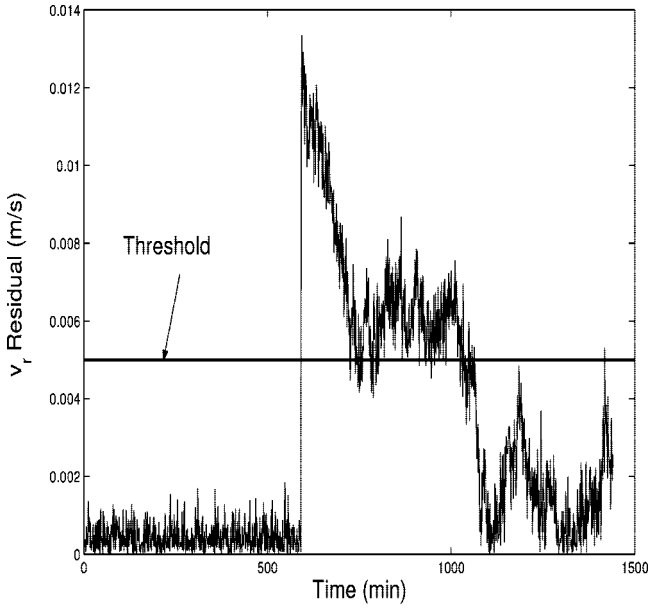

Figure 35. Residual corresponding to the retentate valve versus time. The residual is exceeded at $t = 592$ min.

the alternative of not implementing FDIFTC where the state may move to an undesired region for all time after an actuator fault. For these two simulations, measurements are available continuously, and the control is sample-and-hold every 60 s. It is also assumed that FTC reconfiguration takes place at the next sample and hold interval after detection. A third example displays how FDI performs with sampled measurements that allow for detection but not isolation. The FDIFTC framework allows the resilient operation of the RO system in the presence of valve actuator failures. For this section it is assumed that the fall-back configurations $k = 2$ and $k = 3$ discussed in the FDIFTC section are available for the operator to use.

6.2.1. Failure of the Retentate Valve. For this simulation, the RO system is subjected to a failure in the retentate valve at $t = 35\ 424$ s where the value of e_{v2} gets fixed at 1.4×10^8. The control in this case is nonlinear feedback control with feed-forward compensation as in section 6.1.4. Measurements are assumed to be available continuously, while control is implemented sample-and-hold fashion with a hold time of 60 s. The profiles for retentate velocity, v_r, and pressure, P, with and without FDIFTC recovery can be seen in Figures 24 and 25. It is clear that if no FDI is used, shown by the solid lines in Figures 24 and 25, then the system states move away from the desired set-point values. However, the FDI filters shown in eq 7 can be used with this system to generate residual plots shown in Figures 26 and 27. The sampling time is fast enough to effectively detect and isolate the failure, so only one of the two residuals responds to the fault. It is clear from the residual plots that the failure has occurred in the retentate valve and not in the bypass valve. This actuator fault isolation could not have been done with inspection of the states alone, because both v_b and v_r change significantly upon failure. At the time of detection, $t = 592$ min, the system is switched to the appropriate fall-back configuration under FDIFTC, $k = 2$ in this case, and the system returns to the desired operating point. At the time of detection the FDI filter is initialized at the current state and is ready to detect an actuator failure in the new configuration.

6.2.2. Failure of the Bypass Valve. This example explores a sudden failure in the bypass valve. At $t = 35{,}424$ the bypass valve resistance goes to the nominal value, $e_{v1} = e_{v1}^{ss}$, and is fixed. The profiles of the retentate velocity, v_r, and the pressure, P, with FDIFTC recovery can be seen in Figures 28 and 29.

It is clear that if no FDI is used (solid lines in Figures 28 and 29) then the system states respond, and the system moves to an undesirable operating mode. However, FDIFTC can be implemented to regain control. It can be seen in Figures 30 and 31 that the failure has occurred in the bypass line. According to the FDIFTC switching logic, the system can switch to the fall-back configuration where $k = 3$. This fall-back configuration uses a fall-back bypass valve to replace e_{v1}, and the controller is able to move the system back to the desired operating point. The FDI filter is initialized after reconfiguration to isolate additional actuator failures. The system recovery under FDIFTC can be seen as the dotted lines in Figures 28 and 29.

6.2.3. Failure of the bypass valve; sampled measurements. The final example presents a case where continuous measurements of the system states are not available. Limitations on sampling time are imposed by the dynamic behavior of flow meters and other sensors. Specifically, flow meters have a dynamic response time that can by characterized by a time constant, and the flow signal takes some finite time to adjust to changes in the pipe flow.[28] To this end, sample-and-hold operation, with a sampling time of 60 s, is implemented. The sensor dynamics are assumed to be fast compared to this sampling time and are neglected.

This example includes a sudden failure in the bypass valve; at $t = 35\ 424$ s the bypass valve resistance goes to 1.5×10^8 and is fixed. The profiles of the retentate velocity, v_r, and the pressure, P, with FDIFTC recovery can be seen in Figures 32 and 33. Both states diverge simultaneously due to this failure.

The FDI filters, shown in Figures 34 and 35, cannot isolate the failure. The failure propagates to both states between consecutive measurements, and thus both residuals exceed the threshold so that it is impossible to isolate the failed actuator. However, the FDI filters still provide fault detection, and the operator could take action at the time of detection to examine the system and search for the source of the failure. Even though FDI is impossible with a large sample period for this system, in practice the dynamics of an RO plant may not be as fast as the dynamics of the model proposed in eq 1. Slower system dynamics would allow for FDI filters to perform adequately even under sampled measurements if the sample time is sufficiently fast compared to the system dynamics.

7. Conclusions

The contributions of this work include the development of a dynamic model for high recovery RO desalination. This model describes the spatial and temporal behavior of a high recovery RO desalination process. Additionally, nonlinear control techniques that include feed-forward/feedback control for disturbance rejection and FDIFTC have been applied to this dynamic model accounting for practical issues such as noisy/sampled measurements, large time varying disturbances, and actuator failures. Nonlinear Lyapunov-based feed-forward/feedback controllers were implemented on the high recovery RO system in simulation examples. The additional feed-forward component in the controller was able to compensate for large time varying disturbances in the feed concentration. FDIFTC methods were applied in simulation examples in order to detect actuator faults and switch appropriately to fall-back configurations avoiding undesired RO system operation.

The first set of simulation studies examined the ability of the feed-forward/feedback control algorithms to handle a large time varying disturbance on the feed concentration. These simulations account for such practical issues as sampled measurements and time-varying disturbances. The first feed-forward/feedback control simulation demonstrated the ability to mitigate disturbances with the system states, υ_b and υ_r, as controlled outputs. The pressure, P, in this simulation varied to a large extent (a possible safety concern), and this P variation motivated the application of feed-forward/feedback control with the pressure and retentate velocity, P and υ_r, as controlled outputs. The second feed-forward/feedback simulation demonstrated the ability to mitigate the effect of the disturbance on the system pressure, P. The second set of simulation studies demonstrated the application of FDI and FTC structures to this RO system. These simulations account for such practical issues as sampled noisy measurements and plant/model parameter mismatch. The first FDIFTC simulation demonstrated the detection, isolation, and appropriate switching when the system is subjected to a failure on the retentate valve. The second FDIFTC simulation demonstrated the detection, isolation, and appropriate switching when the system is subjected to a failure on the bypass valve.

Acknowledgment

Financial support from the National Science Foundation, CTS-0529295, and the State of California Department of Water Resources is gratefully acknowledged.

Literature Cited

(1) Abbas, A. Model predictive control of a reverse osmosis desalination unit. *Desalination* **2006**, *194*, 268–280.

(2) Aboabboud, M.; Elmasallati, S. Potable water production from seawater by the reverse osmosis technique in Libya. *Desalination* **2007**, *203*, 119–133.

(3) Alatiqi, I. M.; Ghabris, A. H.; Ebrahim, S. System identification and control of reverse osmosis desalination. *Desalination* **1989**, *75*, 119–140.

(4) Assef, J. Z.; Watters, J. C.; Deshpande, P. B.; Alatiqi, I. M. Advanced control of a reverse osmosis desalination unit. *J. Process Control* **1997**, *7*, 283–289.

(5) Bartman, A.; McFall, C.; Christofides, P. D.; Cohen, Y. Model predictive control of feed flow reversal in a reverse osmosis desalination process. *J. Process Control* **2008**, in press.

(6) Bird, R. B.; Stewart, W. E.; Lightfoot, E. N. *Transport Phenomena*, 2nd ed.; Wiley: New York, 2002.

(7) Burden, A. C.; Deshpande, P. B.; Watters, J. C. Advanced control of a B-9 Permasep permeator desalination pilot plant. *Desalination* **2001**, *133*, 271–283.

(8) Chapra, S. C.; Canale, R. P. *Numerical Methods for Engineers*, 4th ed.; McGraw Hill: New York, 2002.

(9) Chen, J.; Wang, F.; Meybeck, M.; He, D.; Xia, X.; Zhang, L. Spatial and temporal analysis of water chemistry records (1958−2000) in the Huanghe (Yellow River) basin. *Global Biogeochem. Cycles* **2005**, *19*, GB3016.

(10) Christofides, P. D.; El-Farra, N. H. *Control of nonlinear and hybrid process systems: designs for uncertainty, constraints and time delays*; Springer: New York, 2005.

(11) Dickson, J. M.; Spencer, J.; Costa, M. L. Dilute single and mixed solute systems in a spiral wound reserve osmosis module Part I: Theoretical model development. *Desalination* **1992**, *89*, 63–88.

(12) El-Farra, N. H.; Christofides, P. D. Integrating robustness, optimality, and constraints in control of nonlinear processes. *Chem. Eng. Sci.* **2001**, *56*, 1841–1868.

(13) El-Farra, N. H.; Christofides, P. D. Bounded robust control of constrained multivariable nonlinear processes. *Chem. Eng. Sci.* **2003**, *58*, 3025–3047.

(14) Gambier, A.; Badreddin, E. Application of hybrid modeling and control techniques to desalination plants. *Desalination* **2002**, *152*, 175–184.

(15) Gani, A.; Mhaskar, P.; Christofides, P. D. Fault-tolerant control of a polyethylene reactor. *J. Process Control* **2007**, *17*, 439–451.

(16) Geankoplis, C. J. *Transport Processes and Separation Process Principles*, 4th ed.; Prentice Hall: New York, 2003.

(17) Herold, D.; Neskakis, A. A small PV-driven reverse osmosis desalination plant on the island of Gran Canaria. *Desalination* **2001**, *137*, 285–292.

(18) Kimes, J. K. The regulation of concentrate disposal in Florida. *Desalination* **1995**, *102*, 87–92.

(19) Lin, Y.; Sontag, E. D. A universal formula for stabilization with bounded controls. *Syst. Control Lett.* **1991**, *16*, 393–397.

(20) Liu, C. K.; Park, J.-W.; Migita, R.; Qin, G. Experiments of a prototype wind-driven reverse osmosis desalination system with feedback control. *Desalination* **2002**, *150*, 277–287.

(21) Lua, Y.; Hua, Y.; Zhang, X.; Wu, L.; Liu, Q. Optimum design of reverse osmosis system under different feed concentration and product specification. *J. Membr. Sci.* **2007**, *287*, 219–229.

(22) McFall, C. W.; Christofides, P. D.; Cohen, Y.; Davis, J. F. Fault-tolerant control of a reverse osmosis desalination process. *Proceedings of 8th internation IFAC Symposium on Dynamics and Control of Process Systems*, Cancun, Mexico, 2007; Vol. 3, pp 163−168.

(23) Mhaskar, P.; Gani, A.; El-Farra, N. H.; McFall, C.; Christofides, P. D.; Davis, J. F. Integrated fault-detection and fault-tolerant control of process systems. *AIChE J.* **2006**, *52*, 2129–2148.

(24) Mhaskar, P.; McFall, C.; Gani, A.; Christofides, P. D.; Davis, J. F. Fault-tolerant control of nonlinear systems: Fault-detection and isolation and controller reconfiguration. *Proceedings of American Control Conference*, Minneapolis, MN, 2006; pp 5115−5122.

(25) Mhaskar, P.; McFall, C.; Gani, A.; Christofides, P. D.; Davis, J. F. Isolation and handling of actuator faults in nonlinear systems. *Automatica* **2008**, *44*, 53–62.

(26) Ogunnaike, B. A.; Ray, W. H. *Process Dynamics, Modeling, and Control*; Oxford University Press, New York, 1994.

(27) Rahardianto, A.; Gaoa, J.; Gabelich, C. J.; Williams, M. D.; Cohen, Y. High recovery membrane desalting of low-salinity brackish water: Integration of accelerated precipitation softening with membrane RO. *J. Membr. Sci.* **2007**, *289*, 123–137.

(28) Riggs, J. B.; Karim, M. N. *Chemical and Bio-Process Control*, 3rd ed.; Ferret: Lubbock, TX, 2006.

(29) Robertson, M. W.; Watters, J. C.; Desphande, P. B.; Assef, J. Z.; Alatiqi, I. M. Model based control for reverse osmosis desalination processes. *Desalination* **1996**, *104*, 59–68.

(30) Siljak, D. D. Reliable control using multiple control systems. *Int. J. Control* **1980**, *31*, 302–339.

(31) Yang, G. H.; Zhang, S. Y.; Lam, J.; Wang, J. Reliable control using redundant controllers. *IEEE Trans. Autom. Control* **1998**, *43*, 1588–1593.

Received for review November 15, 2007
Revised manuscript received May 28, 2008
Accepted May 29, 2008

IE071559B